Covalent functionalization of single-walled carbon nanotubes by Bingel reaction for building charge-transfer complexes

Olga A. Stasyuk,*[a] Anton J. Stasyuk,[a] Alexander A. Voityuk[a,b] and Miquel Solà*[a]

[a] Institute of Computational Chemistry and Catalysis, University of Girona, C/ M. Aurèlia Capmany, 69, 17003 Girona, Catalonia, Spain

[b] ICREA, Pg. Lluís Companys 23, 08010 Barcelona, Spain

Corresponding Authors

* e-mail: o.a.stasuk@gmail.com

* e-mail: miquel.sola@udg.edu

TOC

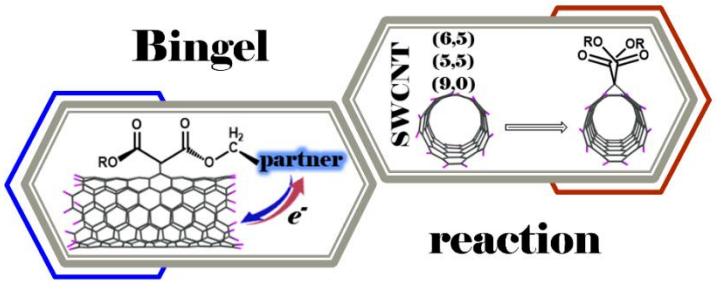

Abstract

Functionalization of nanotubes with donor and acceptor partners by the Bingel reaction leads to formation of charge-transfer dyads, which can operate in organic photovoltaic devices. In this work, we theoretically examine the mechanism of the Bingel reaction for (6,5)-chiral, (5,5)-armchair, and (9,0)-zig-zag single-walled carbon nanotubes (SWCNTs), and demonstrate that the reaction is regioselective and takes place at the perpendicular position of (6,5)- and (5,5)-SWCNTs, and oblique position of (9,0)-SWCNT. Further, we design computationally the donor-acceptor complexes based on (6,5)-SWCNT coupled with partners of different electronic nature. Analysis of their excited states reveals that efficient photoinduced charge transfer can be achieved in the complexes with exTTF, ZnTPP, and TCAQ. The solvent can significantly affect the population of the charge separated states. Our calculations show that electron transfer (ET) occurs in normal Marcus regime on sub-nanosecond time scale in the complexes with exTTF and ZnTPP, and in inverted Marcus regime on picosecond time scale in the case of TCAQ derivative. The ET rate is found to be not very sensitive to the degree of functionalization of the nanotube.

Introduction

Organic photovoltaics (OPVs) is a relatively new and promising area of research due to such their advantages as low cost, light weight and mechanical flexibility[1]. In OPVs, the absorbing material is a thin-layer organic semiconductor that is sandwiched between two electrodes. In order to increase the efficiency of solar cells, it is important to choose a semiconductor material with appropriate properties. Carbon nanotubes are very appealing in this field. However, single-walled carbon nanotubes (SWCNTs) are insoluble in water and organic solvents due to strong π-π interactions and tend to form agglomerates. For this reason, their chemical functionalization is used.[2] Further coupling of functionalized nanotubes with photochromic molecules allows one to

construct novel donor-acceptor materials with advantageous optical and electrical properties.[3,4,5,6] To date, a number of donor-acceptor SWCNT-based hybrids are known, particularly, with porphyrins, ferrocenes, perylene diimides, phthalocyanines, and polyaromatic hydrocarbons.[7,8,9,10,11,12] Photoactive molecules can be attached to the nanotube *via* covalent or noncovalent interactions. Noncovalent functionalization preserves π-electron conjugation of the sp^2 carbon network but it is difficult to provide environmental and long-time stability of systems. In turn, covalent binding is strong, but usually generates sp^3 carbon sites on CNTs, which disrupt the transitions of π-electrons, leading to loss of desired properties.

Insolubility of nanotubes and low charge mobility between donor and acceptor parts can be overcome by functionalization of nanotubes using Bingel cycloaddition reaction.[13] Nowadays, this reaction is successfully applied to fullerenes for their chemical modification.[14,15,16,17,18,19,20] A classical Bingel reaction is a type of nucleophilic addition reaction introducing a cyclopropane on the fullerene cage. Despite a widespread use of this reaction in fullerene chemistry,[21] only a few reports have appeared for the functionalization of SWNTs[22,23] and other carbon materials, such as nanodiamond,[24] graphene[25,26] and carbon nanohorns.[27]

The first example of SWCNTs functionalization *via* the Bingel reaction was reported in 2003 by Coleman and co-workers.[22] They confirmed the successful cyclopropanation of SWNTs by AFM in conjunction with chemical tagging techniques. Later, structures and spectroscopic properties of functionalized SWNTs were examined in detail.[23] Resonant Raman and UV-vis-NIR absorption spectroscopies revealed that the electronic properties of SWNTs are well preserved even after significant degree of sidewall modification by the Bingel reaction.

Results of theoretical investigations of [2+1] cycloaddition reactions are in perfect agreement with experimental findings. The calculations showed that the strain of three-membered ring formed

during the reaction with carbenes or nitrenes leads to sidewall bond cleavage, recovering sp^2 hybridization of two carbon atoms, and thus preserving electronic properties of SWCNTs.[28,29,30,31] It was also found that isomerization between open and closed forms depends strongly on the chirality and curvature of the metallic nanotubes. The open isomer is predominant in high curvature CNTs, whereas in large nanotubes, which are greater that (18,18)-CNT, the closed isomer becomes lower in energy.[32]

The Bingel reaction can be a good approach for functionalization of nanotubes with donor or acceptor partners forming charge-transfer dyads, which can operate in OPV devices. In this work, we studied the mechanism of this reaction for armchair, zig-zag, and chiral SWCNTs, and designed computationally the donor-acceptor complexes based on chiral (6,5)-SWCNT coupled with selected partners of a different electronic nature: tetrathiafulvalene (TTF), its π-extended analogue (exTTF), and zinc tetraphenylporphyrin (ZnTPP) as electron donors, and anthraquinone (AQ) and tetracyanoanthraquinodimethane (TCAQ) as electron acceptors.

Results and discussion

Quantum-chemical modeling of the mechanism of the Bingel reaction for SWCNTs was performed for (6,5)-chiral, (5,5)-armchair, and (9,0)-zig-zag SWCNTs consisting of 3 Clar unit cells ($C_{110}H_{20}$, $C_{108}H_{24}$, and $C_{96}H_{22}$, respectively). The donor-acceptor complexes were designed by using 5 Clar unit cells ($C_{160}H_{22}$) in the model of (6,5)-SWCNT. The Clar cell model of a SWCNT[33] is a fully benzenoid structure with closed-shell singlet ground state. Clar models of SWCNT guarantee faster convergence of electronic properties with the model length.

Depending on the type of nanotube, the formation of cycloadduct with bromomalonate can take place *via* attacks to different carbon atoms forming products with parallel (***par***), perpendicular

(***per***) or oblique (***obl*** and ***obl2***) orientation with respect to the nanotube axis. The Clar unit cells and different available reaction sites for the studied reaction are depicted in Figure 1.

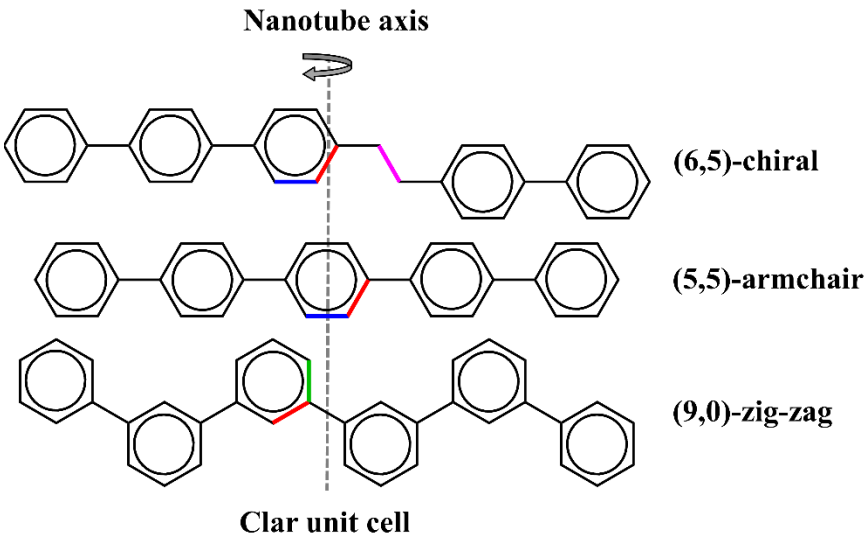

Figure 1. Clar unit cell of the studied SWCNTs and non-equivalent C-C bonds relative to the nanotube axis: ***per*** (blue), ***obl*** (red), ***par*** (green), and ***obl2*** (magenta).

Mechanism of the Bingel reaction

In the first reaction step, the base abstracts the acidic proton of the bromomalonate to generate a carbanion. Then, it attacks the nanotube forming a carbanion intermediate with negative charge on the nanotube. In the final step, the intermediate undergoes the three-membered ring closure with displacement of the bromide (Scheme 1). Since an initial attack on the C-C bond of the nanotube can be carried out from different sides, adjacent carbon atoms were denoted as C_α and C_β, and all stationary points related with these positions were labeled with subscript α or β.

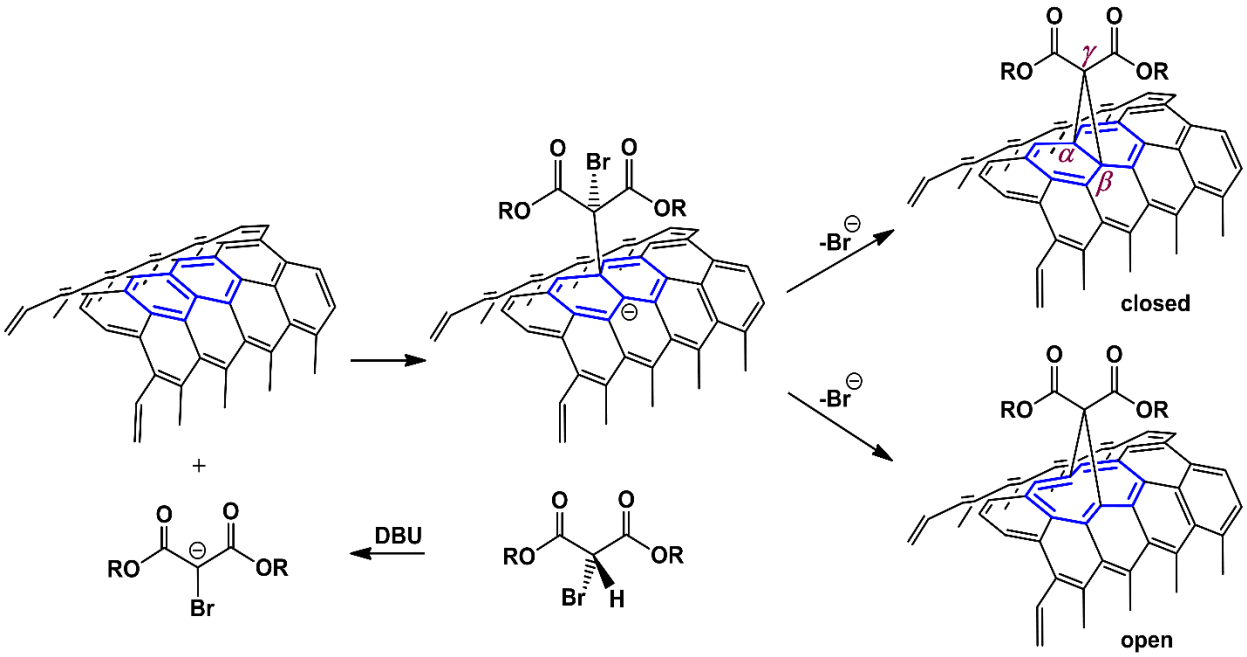

Scheme 1. General mechanism of the Bingel reaction for SWCNTs.

Thus, we will consider two reaction pathways, with the initial attack on the C_α or C_β, for each non-equivalent C_α–C_β bond leading to the cycloadduct in open form with $d(C_\alpha–C_\beta) \approx 2.20$ Å or closed form with $d(C_\alpha–C_\beta) \approx 1.57$ Å (Table 1). The products with open cyclopropane bridge are regularly more stable than their closed analogs. In the case of C_{60}, an open [5,6] cycloadduct is formed, whereas for [6,6] bonds the closed isomer is favored.[34] This behavior is caused by the deformation energy difference. It is much easier to deform a [5,6] bond in C_{60} to make it opened than a [6,6] bond, because the former is longer and has a smaller double bond character.[35] For (6,5)- and (5,5)-SWCNTs, the open product is formed in perpendicular orientation of cyclopropane ring, whereas for (9,0)-SWCNT it is built when the bridge is in oblique position to the nanotube axis. Selective formation of the open adducts with the binding configuration perpendicular to the nanotube axis was also found for (8,8)- and (10,5)-SWCNTs in an earlier computational study.[36] Therefore, this reaction can lead to the nanotubes functionalized in the position different from the observed in the

[4+2] or [2+2] cycloaddition reactions,[37,38] and in the Pauson-Khand reaction.[39] Moreover, the experimental study on the sidewall functionalization of HiPco SWNTs using the Bingel reaction showed that the degree of the sidewall functionalization (one group per 75-300 carbon atoms of SWNTs) can be controlled by changing the output power of microwave heating.[23]

Table 1. Selected characteristics for possible Bingel products of SWCNTs.

Position of cycloaddition	ΔE_{rel}, kcal/mol	ΔG_{rel}, kcal/mol	$d(C_\alpha–C_\beta)^{ini}$,[a] Å	$d(C_\alpha–C_\beta)$, Å	Angle ($C_\alpha C_\gamma C_\beta$), °	Type of cycloadduct
(6,5)-SWCNT						
per	0.0	0.0	1.417	2.183	93.3	open
obl	19.2	18.5	1.424	1.566	62.3	closed
obl2	16.8	16.9	1.416	1.565	61.9	closed
(5,5)-SWCNT						
per	0.0	0.0	1.430	2.217	94.9	open
obl	26.2	25.5	1.422	1.569	62.1	closed
(9,0)-SWCNT						
par	8.2	5.3	1.414	1.527	60.7	closed
obl	0.0	0.0	1.435	2.198	94.4	open

[a] $d(C_\alpha–C_\beta)^{ini}$ refers to the initial $C_\alpha–C_\beta$ bond in the pristine SWCNTs

(6,5)-chiral SWCNTs

Gibbs energies in toluene for the formation of intermediates (Int), transition states (TS) and cycloaddition products (P) relative to the separated reactants (pristine nanotube + dimethyl bromomalonate) are shown in Figure 2. Dimethyl bromomalonate was taken instead of diethyl

bromomalonate used in the experiment[22] to simplify the theoretical model. Taking into account non-equivalent C-C bonds in (6,5)-SWCNT, three products are possible: ***per***, ***obl*** and ***obl2***. There are two possible reaction pathways leading to each product: (i) first goes through Int_{α} and TS_{α}; (ii) second follows the formation of Int_{β} and TS_{β}. In all cases, the geometries of Int_{α} and Int_{β} are very similar. Thus, we can observe two cases depending on the relative stability of Int and P. In the first case, when the product is more energetically stable than Int_{α} and Int_{β} both reaction pathways will lead to the formation of the cyclopropanated CNT. This case is realized when reaction takes place in ***per*** position. The formation of the Bingel product ($\Delta G(P_{per})$ = -10.8 kcal/mol) with open cyclopropane bridge is more preferred that the formation of the intermediates by 9.1 and 10.5 kcal/mol. The reaction proceeds with energy barrier of 21-23 kcal/mol. When attacking the ***obl2*** position, bromomalonate forms stable intermediates with nanotube ($\Delta G(Int_{obl2}) \approx$ -6 kcal/mol). In such case, when both intermediates, Int_{α} and Int_{β}, are energetically more favorable with respect to the product, the reaction will not lead to the cycloadduct despite the lower energy barrier than for the ***per*** product. This case is observed during the formation of ***obl*** or ***obl2*** products with energy barriers between 13 and 15 kcal/mol. For the ***obl*** position, the product is less stable than the intermediates by 7.8 and 6.8 kcal/mol, whereas for the ***obl2*** position this difference is 12.3 and 12.5 kcal/mol. Their destabilization are most likely explained by formation of closed three-membered ring on the side of nanotube with high ring strain ($d(C_{\alpha}–C_{\beta})\approx$1.57Å, angle($C_{\alpha}C_{\gamma}C_{\beta}$)=62°). Thus, we can conclude that during the Bingel reaction in (6,5)-SWCNTs the only product with the perpendicular orientation of the cyclopropane bridge with respect to the nanotube axis can be formed with the energy barrier accessible under mild conditions. Along with this product, two singly bonded derivatives corresponding to the intermediates for ***obl2*** position can be also observed experimentally. Prevalence of the thermodynamically favorable open product

in ***per*** position with higher energy barrier was previously reported for functionalization of (10,5)-SWCNT.[36]

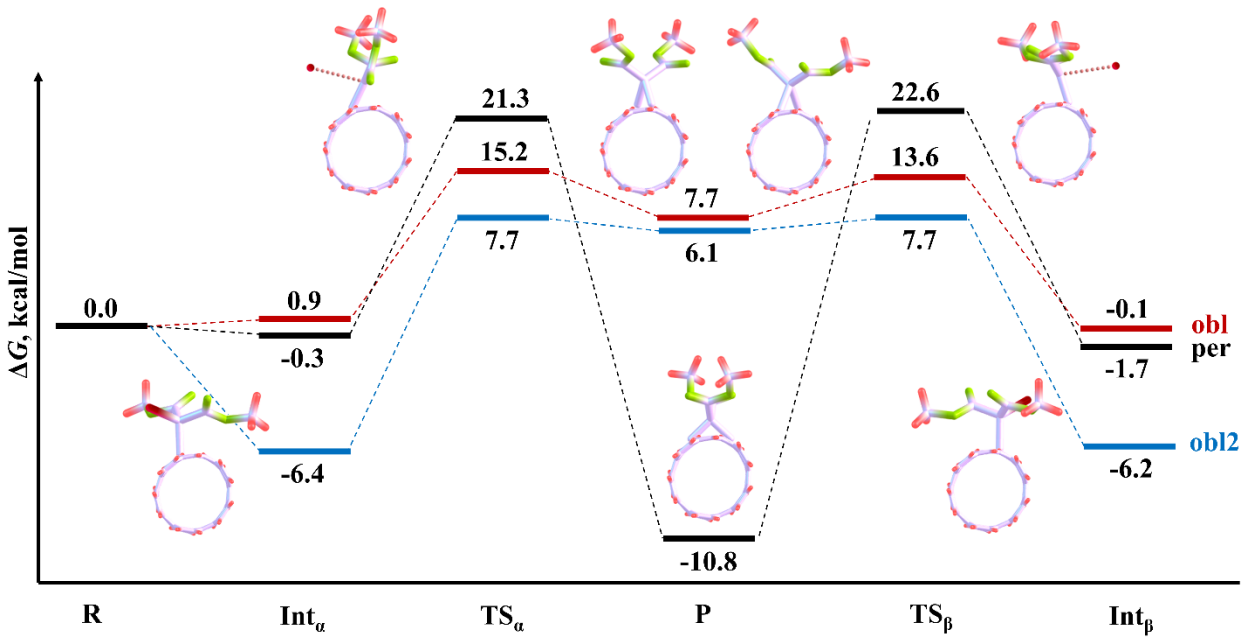

Figure 2. Gibbs energy profiles of the Bingel reaction in toluene for (6,5)-SWCNT with formation of a cycloadduct in perpendicular (***per***, black) or oblique (***obl***, red and ***obl2***, blue) orientations with respect to the nanotube axis.

(5,5)-armchair SWCNTs

For (5,5)-SWCNT, the reaction proceeds *via* two intermediates (Int$_\alpha$ and Int$_\beta$) when bromomalonate interacts with a nanotube. As in previous case, the reaction can start from two different sides of C-C bond, C$_\alpha$ and C$_\beta$. Orientation of bromomalonate with respect to the nanotube to form ***per*** or ***obl*** products does not change much the stability of the intermediates, which are more stable by 7-10 kcal/mol than the reactants (Figure 3). Stable intermediates were previously observed for (8,8)-SWCNT using B3PW91 functional, whereas B3LYP results indicated that the

energy of Int is comparable to the energy of the reactants.[36] The following formation of the ***per*** product goes through TS_α or TS_β with energy barriers of 22.2 and 24.9 kcal/mol, respectively. In turn, the formation of the ***obl*** product requires lower energy, in particular 15 and 19.4 kcal/mol to reach TS_α and TS_β. However, high angle and torsional strains of the formed cyclopropane ring in the ***obl*** product make it lower stable than the intermediates (Table 1). In general, energy barriers that lead to open adducts are higher because the bond attacked needs to be stretched to a greater extent. This result is also supported by energy profiles computed for (8,8)-SWCNT.[36] The obtained results indicate that for (5,5)-SWCNT the Bingel reaction leads to the stable singly bonded intermediates and ***per*** product with open cyclopropane bridge, which is very similar to (6,5)-SWCNT.

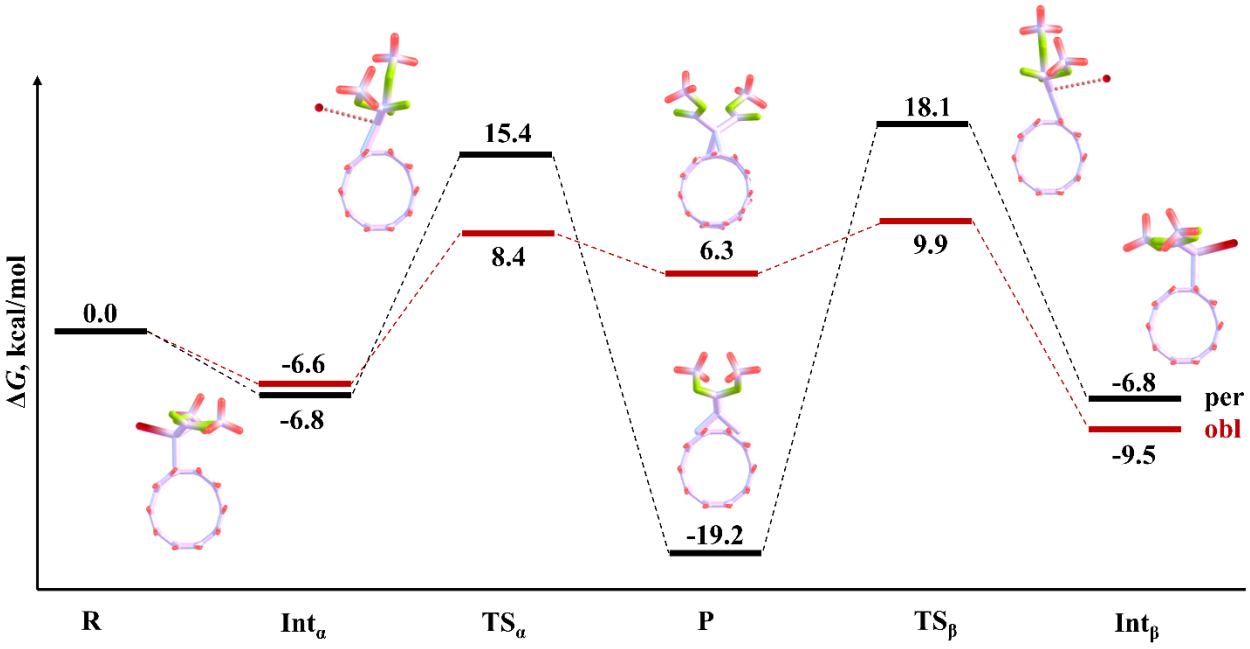

Figure 3. Gibbs energy profiles of the Bingel reaction in toluene for (5,5)-SWCNT with formation of a cycloadduct in perpendicular (***per***, black) or oblique (***obl***, red) orientations with respect to the nanotube axis.

(9,0)-zig-zag SWCNTs

The mechanism of the Bingel reaction for (9,0)-SWCNT is similar to the previously considered for (6,5)- and (5,5)-SWCNTs. A distinctive feature of this type of nanotubes is a possibility of formation of the reaction product with parallel orientation of cyclopropane bridge with respect to the nanotube axis, in addition to the oblique one. For example, the sidewall (4 + 2) cycloaddition reaction of zig-zag SWCNTs leads to the addition of benzyne in the parallel position to the SWCNTs axes.[37] The parallel product is also formed in the [2 + 2 + 1] cycloaddition Pauson-Khand reaction.[39] The computed Gibbs energies of all stationary points for the formation of ***par*** and ***obl*** products of the Bingel reaction are presented in Figure 4. In contrast to (6,5)- and (5,5)-SWCNTs, the preferable product of the (9,0)-SWCNT cyclopropanation is the ***obl*** product with open cyclopropane bridge ($d(C_\alpha–C_\beta)$=2.20Å). The reaction starts from creation of singly bonded intermediates at C_α or C_β positions. Int_α and Int_β are more stable than reactants by 5 kcal/mol. Then they need to overcome the energy barrier of 26 kcal/mol to from the ***obl*** product, which is a slightly more favored than the intermediates. The relative energetic stabilities of intermediates and product for the reaction in ***par*** position suggest that the (9,0)-SWCNT cannot be experimentally cycloprotonated in ***par*** position, because P_{par} is higher in energy than Int_α and Int_β. Interestingly, Int_α for ***par*** position is energetically comparable with the ***obl*** product.

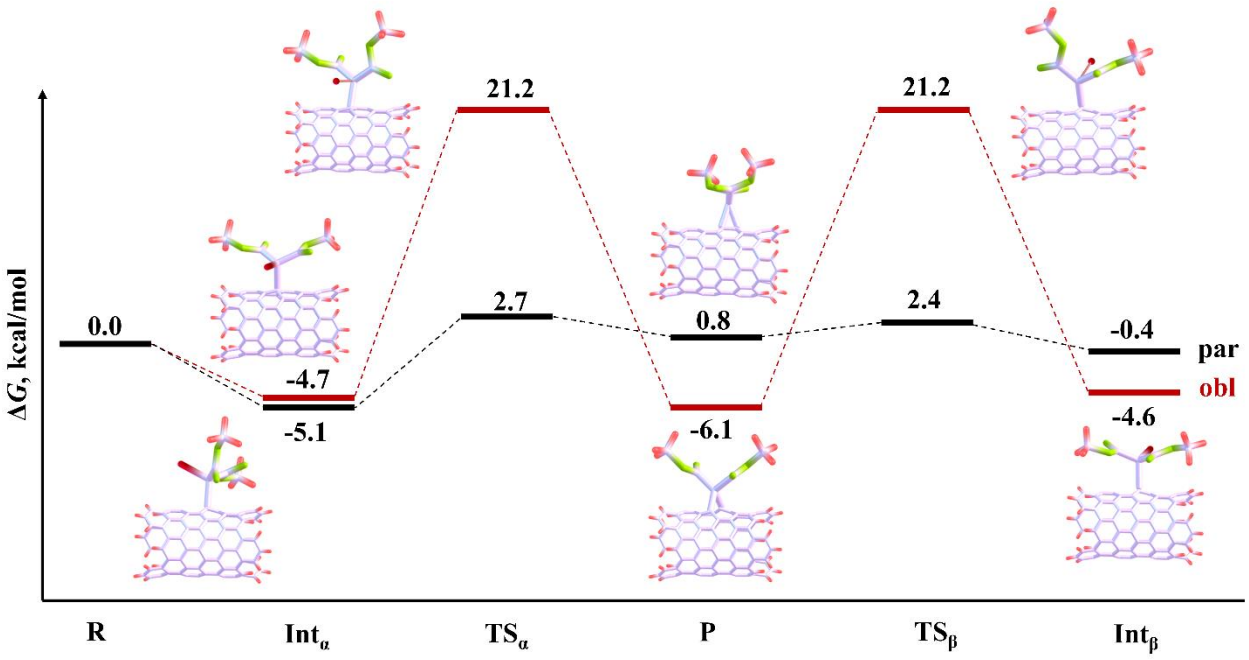

Figure 4. Gibbs energy profiles of the Bingel reaction in toluene for (9,0)-SWCNT with formation of a cycloadduct in parallel (***par***, black) or oblique (***obl***, red) orientations with respect to the nanotube axis.

Complexes with electron donor and electron acceptor molecules

We designed several donor-acceptor complexes of (6,5)-SWCNTs, because enriched semiconducting (6,5)-SWCNTs are commercially available and according to the Gibbs energy profile are more reactive in the Bingel reaction than (5,5)- and (9,0)-SWCNTs. It can be expected that functionalization of the enriched (6,5)-SWCNTs will be more efficient than that of standard HiPco SWCNTs[22,23] because of a lower energy barrier required to produce an open cycloadduct for (6,5)-SWCNTs compared to other types of nanotubes. However, further experimental studies are needed to prove this. In Raman spectra, the ratio between D and G bands reflecting a fraction of sp^3 carbon atoms[40] is expected to be similar to that in the pristine material. This will indicate that no conversion of sp^2 to sp^3 carbon atoms occurs. However, some increase in the D/G ratio can be observed due to formation of stable singly bonded intermediates.

Note that in donor-acceptor dyads, (6,5)-SWCNT can act either as an efficient electron donor or electron acceptor depending on the partner. Let us consider several (6,5)-SWCNT dyads with typical donor and acceptor moieties attached through the Bingel reaction. As a typical electron acceptor, we took anthraquinone (AQ) and its derivative 11,11,12,12-tetracyano-9,10-anthraquinodimethane (TCAQ). As electron donor, we considered tetrathiafulvalene (TTF), its π-extended analogue 9,10-di(1,3-dithiol-2-ylidene)-9,10-dihydroanthracene (exTTF), and zinc tetraphenylporphyrin (ZnTPP). These molecules are shown in Figure 5 and their HOMO/LUMO energies are listed in Table 2. It is worth noting that very similar HOMO and LUMO energies of the pristine and functionalized SWCNT indicate that the π-electron system of the pristine species is well-preserved in the open adducts. This agrees well with the experimental data that the electronic properties of SWNTs are maintained after sidewall modification by the microwave-assisted Bingel reaction,[23] and with theoretical findings that the open cycloadduct affects only slightly the orbital energies of the pristine nanotubes.[36]

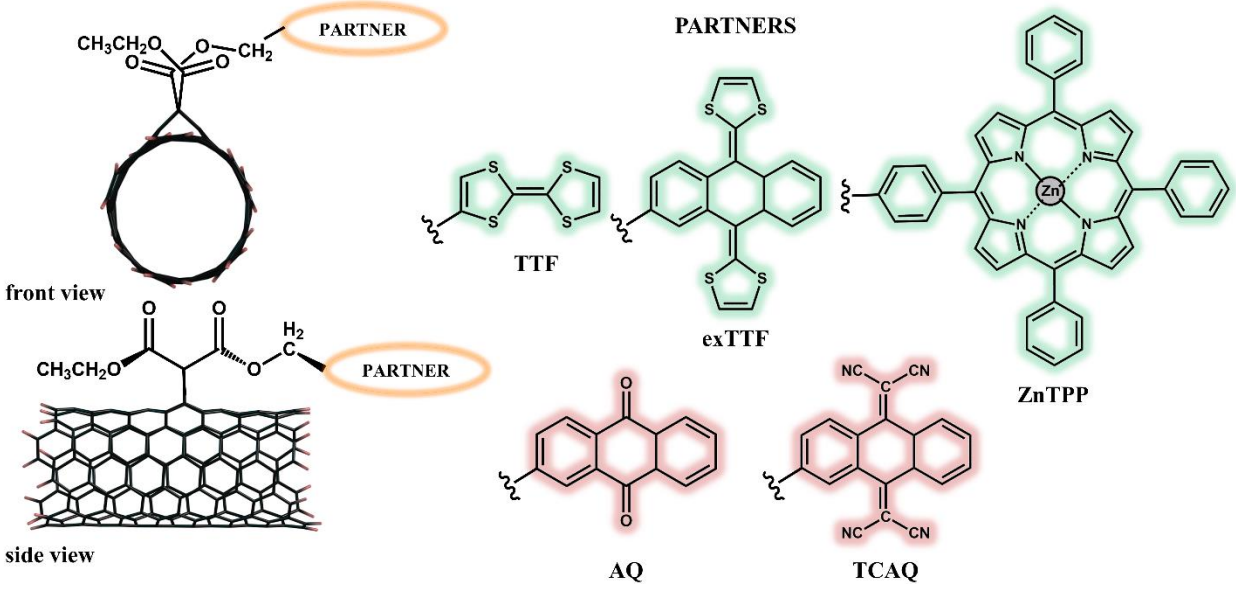

Figure 5. Donor-acceptor complexes of (6,5)-SWCNT with different partners (electron donors are marked with green and electron acceptors with red).

Table 2. Energies of HOMO and LUMO for (6,5)-SWCNT and electron donor and electron acceptor partners at the CAM-B3LYP/def2SVP level of theory.

Molecule	HOMO, eV	LUMO, eV	Δ|HOMO-LUMO|, eV	Electronic property
pristine SWCNT	-5.54	-2.41	3.13	donor or acceptor
functionalized SWCNT	-5.58	-2.45	3.13	donor or acceptor
TTF	-5.89	0.54	6.44	donor
exTTF	-6.13	-0.53	5.60	donor
ZnTPP	-6.19	-1.71	4.48	donor
AQ	-8.80	-1.95	6.85	acceptor
TCAQ	-8.43	-2.65	5.78	acceptor

First, we checked a 3 Clar cell model of the nanotube and found that a substituent can interact with the end of the nanotube (Figure S1 in SI) leading to an artificial structure. To avoid this end effect we extended our model to 5 Clar cells. Next, we studied different orientations of the partner molecules in the (6,5)-SWCNT-TTF complex (Figure S2 in SI). Structures with TTF curved around the nanotube are found to be most stable due to stronger interaction with the nanotube surface. This is also true for other partner molecules with the exception of ZnTPP, the planar structure of which is difficult to deform (Figure 6). In addition, we checked if the partner molecule can affect a relative stability of functionalized nanotube isomers. We compared the complexes with ***per*** and ***obl*** functionalization positions, and found that for all donor-acceptor complexes the ***per*** isomers are energetically more favorable than the ***obl*** isomers at least by 10 kcal/mol (Table

S1 in SI). Because of that, we studied electron transfer (ET) processes only in the most stable per isomers.

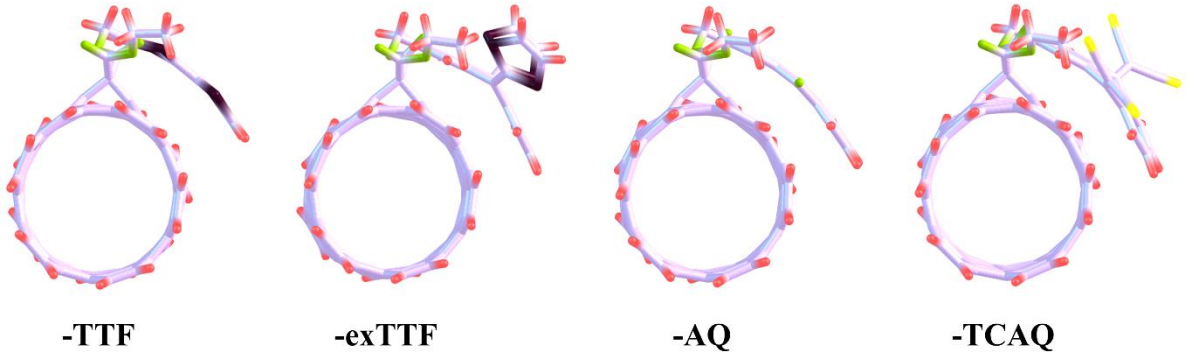

Figure 6. Complexes of (6,5)-SWCNT with curved partner molecules .

Singlet excited states

In order to describe the nature of excited states, each complex was divided into two fragments: (6,5)-SWCNT including cyclopropane bridge, and electron-donating or electron-accepting partner. Exciton delocalization and charge transfer (CT) contributions were analyzed for the 50 lowest excited states of each complex. Three types of excited states were identified: locally excited states (LE) where exciton is mostly localized on single fragment (charge separation value <0.1e); CT states with electron density transferred between two fragments (charge separation >0.9e); and mixed states with significant contributions of both LE and CT (charge separation is between 0.1e and 0.9e).

50 lowest singlet excited states computed for each complex in the gas-phase belong to the energy range of 1.6 to 3.5 eV (Table 2). In all systems, the lowest LE state is found on (6,5)-SWCNT. Its excitation energy is computed to be ~1.76 eV with an exception for TCAQ, 1.94 eV. The LE state on ZnTPP lies by 0.58 eV higher in energy, whereas LE states on other partners are

not found within the considered excited states. The most intense absorption with the oscillator strength from 1.39 to 1.58 is due to electronic transitions in (6,5)-SWCNT.

There are two types of CT states: (i) with electron transfer from a partner molecule to (6,5)-SWCNT (CT1), and (ii) with opposite direction of electron transfer, i.e. from (6,5)-SWCNT to the partner (CT2). The energy of CT states is determined by the electron-donating or accepting nature of (6,5)-SWCNT and the partner, as well as by the ability of these fragments to efficiently delocalize the separated hole-electron pair. The excited states (Table 2) can be divided into 3 groups. Group 1 includes 2 complexes with TTF and exTTF, for which only the CT1 is observed. Group 2 contains the AQ and TCAQ complexes with states of CT2-type. Finally, Group 3 includes the ZnTPP complex where both CT1 and CT2 states of similar energy are found.

Table 2. Excitation energies (E_X, eV), major single-electron excited configuration (HOMO(H)–LUMO(L)) and its weight (W), oscillator strength (f), charge separation (CS), charge transfer (CT) and exciton localization (χ) quantities

	(6,5)-SWCNT – Partner				
	Partner				
	TTF	exTTF	ZnTPP	AQ	TCAQ
	LE1 ((6,5)-SWCNT)				
E_x, eV	1.756	1.757	1.760	1.772	1.935
transition (W)	H – L+1 (0.48)	H – L+1 (0.46)	H – L+1 (0.51)	H – L+1 (0.46)	H – L+1 (0.77)
f	< 0.001	0.002	0.001	0.003	0.014
χ	0.989	0.986	0.994	0.977	0.921
	LE2 (Partner)				
E_x, eV	n/f	n/f	2.337	n/f	n/f

transition (W)			H-2 – L+2 (0.56)		
f			0.036		
χ			0.998		
Most absorptive transition ((6,5)-SWCNT)					
E_x, eV	2.797	2.794	2.795	2.810	2.823
transition (W)	H-6 – L (0.35)	H-4 – L (0.33)	H-4 – L (0.33)	H-3 – L (0.36)	H-3 – L+1 (0.41)
f	1.575	1.523	1.575	1.388	1.424
χ	0.981	0.957	0.992	0.963	0.927
CT1 (Partner → (6,5)-SWCNT)					
E_x, eV	2.542[a]	2.640	3.115		
transition (W)	H-2 – L (0.19)	H-2 – L (0.70)	H-2 – L+1 (0.95)	n/f[b]	n/f[b]
f	0.011	0.115	< 0.001		
CS/CT	0.39/0.40	0.90/0.90	0.99/1.00		
CT2 ((6,5)-SWCNT → Partner)					
E_x, eV			3.176	2.338*	1.599
transition (W)	n/f[b]	n/f[b]	H – L+4 (0.91)	H – L+2 (0.62)	H – L (0.60)
f			0.001	0.135	0.026
CS/CT			1.00/1.00	0.38/0.38	0.89/0.90

[a] State with significant contributions of LE and CT and formally should be considered as mixed state. [b] n/f – states of interest are not found within considered number of excited states.

CT states in group 1 are found at 2.54 and 2.64 eV for complexes with TTF and exTTF, respectively. These states can be described as HOMO-2 to LUMO transition (Figure S3, SI). In the TTF derivative, 0.4 e is transferred from TTF to (6,5)-SWCNT. It is a mixed state with a significant contribution of LE. In the exTTF derivative, almost complete charge transfer occurs – CS value is 0.9e. A similar situation is found for group 2. In the AQ complex, only 0.38 e is transferred whereas a complete CT is predicted in the TCAQ derivative. This CT state is the lowest

excited state of the (6,5)-SWCNT-TCAQ complex. In the ZnTPP complex, CT1 (HOMO-2 → LUMO+1) and CT2 (HOMO → LUMO+4) are characterized by complete electron transfer (Figure S3, SI).

Solvent effects

It is widely accepted that solvation may significantly influence both ground and excited states. Usually, the solvation effect is relatively weak for LE states, whereas CT states are strongly stabilized by a polar solvent.[41] In order to assess the solvent effects, a COSMO-like solvation model with dichloromethane (DCM) as a solvent was applied. The dependence of photoinduced ET processes on the environment were recently reported for covalent donor-acceptor complexes of fullerene.[42,43,44,45] The dipole moment of the studied complexes in the ground state varies from 1.28 to 7.12D. Despite the difference in dipole moments, the complexes have similar solvation energies ranging from -0.41 to -0.51 eV. Note that the fragments are electrically neutral in the ground state of the complexes.

In LE states, the overall picture is similar to that in the ground state. The LE transition energies remain almost unchanged by passing from the gas phase to solution. The dipole moment difference between the LE and GS states is found to be less than 1.0D, regardless of the complex. In the ZnTPP derivative, a similar situation is found also for LE2 excitation, $\Delta\mu^{LE2}$ is 0.15D. Detailed data for all complexes are given in Table S2, SI.

As expected, changes in the dipole moments associated with CT excitations are significantly larger compared to the LE transitions. The largest values of $\Delta\mu^{CT1}$=59.3D and $\Delta\mu^{CT2}$=62.3D were observed for (6,5)-SWCNT-ZnTPP complex. Smaller values are found for the exTTF ($\Delta\mu^{CT1}$ = 33.8D) and TCAQ ($\Delta\mu^{CT2}$ = 26.0D) derivatives. The smallest values of $\Delta\mu^{CT1}$ and

$\Delta\mu^{CT2}$ were observed for TTF ($\Delta\mu^{CT1}$ = 13.6D) and AQ ($\Delta\mu^{CT2}$ = 13.8D) complexes. This large range of $\Delta\mu$ is directly related to an extent of charge transfer between the fragments. In the ZnTPP complex, both CT1 and CT2 states are characterized by complete electron transfer. In the exTTF and TCAQ complexes, CT is about 0.9 e, whereas it does not exceed 0.4 e in the TTF and AQ derivatives. Solvation data for all complexes are collected in Table S2, SI. Figure 7 shows the GS, LE, and CT energies for the lowest lying singlet excited states in the gas phase and DCM solution.

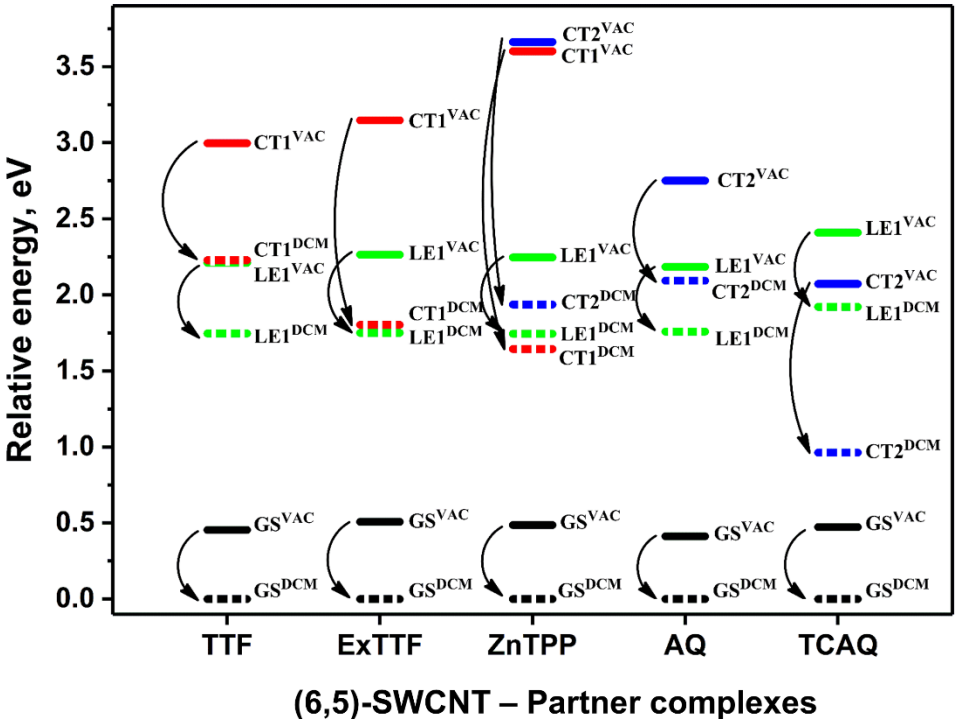

Figure 7. Relative energies (in eV) of the ground state (GS), the first LE state (LE1), and the CT states (CT1, CT2) for the TTF, exTTF, ZnTPP, AQ, and TCAQ derivatives of (6,5)-SWCNT computed in the gas phase (VAC) and dichloromethane (DCM).

As seen from Figure 7, the GS and LE states are stabilized similarly by solvent. The solvation energy of the CT states is sensitive to the dipole moments (it should be is proportional to $\Delta\mu^2$). The solvent stabilization of CT states in the TTF and AQ derivatives are relatively small and the LE1 state remains the lowest one in solution. The solvent effect is significantly stronger in the exTTF and TCAQ complexes. In the ZnTPP derivative, the closely lying CT1 and CT2 states becomes split by passing from the gas phase to solution (the solvation energy is estimated to be -1.96 and -1.73 eV for CT1 and CT2, respectively). The difference in solvation is associated with distinct charge localization. In particular, the charge is more localized in the CT1 state as compared to CT2. Stabilization of CT1 state is strong enough to shift it below LE1, while CT2 remains still higher than the LE1 state.

Electron transfer rates

The absorption of light by a system leads to the generation of excited states, which interconvert extremely fast to the lowest lying excited state. The oscillator strength of CT states in the studied complexes is very weak preventing their direct population. The CT1 or CT2 states can be generated by the decay of the LE1 state when the CT states have a similar or lower energy than the LE1 state. The rate of electron transfer is controlled by three parameters: the electronic coupling V_{ij} between the initial LE and the final CT states; the reorganization energy λ, and the Gibbs energy of the reaction ΔG_0. The reorganization energy is usually divided into two parts, $\lambda = \lambda_i + \lambda_s$, including the internal and solvent terms. The internal reorganization energy λ_i for ET process corresponds to the energy required to deform neutral-state geometries of fragments to charged-state geometries – anion and cation radicals, respectively. The solvent reorganization energy is the energy required to move solvent molecules from positions they occupy in the GS to the locations they will have in

the CT state but without charge transfer. The λ_s for particular CT states is computed as a difference between equilibrium and non-equilibrium solvation energies.

Using computed data listed in Table 3, we estimated ET rates for charge separation (CS) in the exTTF, ZnTPP, and TCAQ complexes. Since the ET processes in the TTF and AQ derivatives are thermodynamically unfavorable (ΔG^0 = 0.48 and 0.34 eV, respectively), their ET rates were not calculated.

Table 3. Electron transfer parameters and ET rates for charge separation (CS) reactions in complexes of (6,5)-SWCNT (DCM solvent).

Complex of (6,5)-SWCNT	Type	ΔG^0, [a] eV	$\|V_{ij}\|$, eV	Reorganization energy λ, eV	Rate constant k_{ET}, sec^{-1}
-exTTF	LE1 $\rightarrow$ CT1	0.012	0.0046	0.381	$1.12 \cdot 10^{10}$
-ZnTPP	LE1 $\rightarrow$ CT1	-0.101	0.0023	0.361	$2.39 \cdot 10^{10}$
	LE1 $\rightarrow$ CT2	0.192	0.0021	0.336	$3.98 \cdot 10^{7}$
-TCAQ	LE1 $\rightarrow$ CT2	-0.958	0.0807	0.525	$4.68 \cdot 10^{12}$

[a] the free energy difference between the final and the initial states in solution.

The photoinduced ET from exTTF and ZnTPP to (6,5)-SWCNT (CT1) occurs in the normal Marcus regime ($|\Delta G^0| < \lambda$). The rates is predicted to be on the sub-nanosecond time scale. Unlike CT1, ET from (6,5)-SWCNT to TCAQ (CT2) takes place in the inverted Marcus regime ($|\Delta G^0| > \lambda$). Its rate is found on the picosecond timescale. Charge separation leading to CT2 in the ZnTPP complex is much slower because of its slightly negative driving force.

Effect of functionalization degree on electron transfer

A degree of sidewall functionalization of HiPco SWNTs by the Bingel reaction is found to be low at room temperature (one diester unit forms per 300 carbon atoms of the SWNT sidewall within 24 h).[23] However, it can be increased using microwave irradiation. One diester unit can be introduced per 140 and even per 75 carbon atoms of SWNT with irradiation power of 50 and 60 W, respectively.

To get more insight into the effect of the degree of sidewall functionalization of SWCNTs on the electron transfer processes, we considered a series of TCAQ coupled with (6,5)-SWCNT of different length because this donor-acceptor complex has quite fast charge separation (on picosecond timescale). To simulate systems with different degrees of functionalization, we gradually increased the length of the nanotube by 2 units, from 5 to 11 Clar unit cells. The smallest system can be consider as a model with a high degree of the functionalization (one group per 160 carbon atoms of the SWCNT), whereas the largest system contains one group per 352 carbon atoms (low degree of functionalization). In each model, we extended the nanotube by 1 Clar cell on each side and did not change the relative position of TCAQ.

First, we examined the influence of the system size on its electronic properties. Let us consider the dependence of the HOMO and LUMO energies (located on SWCNT and TCAQ, respectively), and the HOMO-LUMO gap on the number of Clar cells (Table S3). Increasing the length of the nanotube only slightly influences the electronic properties of the donor-acceptor complex. The HOMO and LUMO energies show a slight increase or decrease, respectively, which leads to a monotonous decrease in the HOMO-LUMO gap, similar to the pristine nanotube.[33] The change in the HOMO-LUMO gap is less than 0.2 eV when going from the 5 to 11 Clar cells model. Then, we performed excited state calculations for the systems. The properties of several relevant excited states are given in Table 4. When going from the smallest (5 Clar cells) to the largest (11

Clar cells) system, the energy of an excited state LE1 (located on nanotube) decreases by 0.14 eV, whereas the energy of the CT2 state increases by the same amount. The degree of charge separation decreases with increasing length of the nanotube, from 0.9**e** in 5 Clar cells model to 0.7**e** in 11 Clar cells model.

Table 4. Excited states properties and the rate of charge separation in the (6,5)-SWCNT-TCAQ complex in DCM

	(6,5)-SWCNT-TCAQ			
	5 Clar cells	7 Clar cells	9 Clar cells	11 Clar cells
	LE1 ((6,5)-SWCNT)			
E_x, eV	1.922	1.900	1.848	1.783
Transition (W)	H – L+1 (0.77)	H – L+1 (0.79)	H – L+1 (0.55)	H – L+1 (0.40)
f	0.014	1.210	1.898	2.495
χ	0.921	0.988	0.990	0.984
	CT2 ((6,5)-SWCNT $\rightarrow$ TCAQ)			
E_x, eV	0.963	0.971	1.055	1.101
Transition (W)	H – L (0.60)	H – L (0.61)	H – L (0.61)	H – L (0.61)
f	0.026	0.028	0.073	0.190
CS/CT	0.89/0.90	0.81/0.81	0.76/0.76	0.72/0.72
	ET parameters and rates			
$\Delta G^0 = E_{CS} - E_{LE}$, eV	-0.958	-0.929	-0.793	-0.682
$\lvert V_{ij} \rvert$, eV	0.0807	0.0456	0.0484	0.0223
Reorganization energy λ, eV	0.525	0.514	0.473	0.448
Rate constant k_{ET}, sec^{-1}	$4.68 \cdot 10^{12}$	$1.87 \cdot 10^{12}$	$6.96 \cdot 10^{12}$	$2.55 \cdot 10^{12}$

Finally, we calculated the rate of the ET reaction as a function of the number of Clar cells. In all cases, the ET occurs on the picosecond timescale. The observed changes in the ET rate are quite small as a decrease in the ($\Delta G^0+\lambda$) term in the Marcus equation (Eq. S7), which would increase the rate, is compensated by decreasing electronic coupling $|V_{ij}|$. Thus, we propose that even with a low degree of functionalization, an efficient population of the CT state should be possible.

Conclusions

The Bingel reaction on nanotubes leads to the formation of three-membered ring on their sidewall. We have studied the reaction mechanism for three types of nanotubes. It has been suggested that chiral (6,5)-SWCNTs are more reactive than armchair and zig-zag nanotubes. The energy barrier required to functionalize (6,5)-SWCNT is 21-23 kcal/mol, whereas for (5,5)- and (9,0)-SWCNTs it amounts to 22-25 and 26 kcal/mol, respectively.

The isomers with open cyclopropane bridge are found to be more stable than their closed analogs. The Bingel reaction is regioselective and takes place particularly at the perpendicular position of (6,5)- and (5,5)-SWCNTs and oblique position of (9,0)-SWCNT. In addition, singly bonded intermediates are well stabilized and even compete with the ***obl*** product in zig-zag nanotubes.

In donor-acceptor complexes, (6,5)-SWCNT can act as electron donor or acceptor depending on the partner. The solvent effect is crucial for the effective population of charge separated states. The efficient photoinduced charge transfer was found in the complexes with exTTF, ZnTPP, and TCAQ. For ZnTPP, charge transfer may occur in both directions, either from CNT to ZnTPP or from ZnTPP to CNT. The last process is shown to be faster in DCM. In the complexes with exTTF and ZnTPP, electron transfer takes place in the normal Marcus regime on sub-nanosecond time scale, whereas in the TCAQ derivative, the electron transfer reaction occurs in the inverted Marcus regime on the picosecond time scale. No significant effect of the nanotube length on the ET rate was found.

Experimental Section

Computational Methods

DFT calculations were carried out using the ADF (Amsterdam Density Functional) program[46] and QUILD code.[47] Geometries of the reactants, intermediates, transition states and products were optimized without any constraints using BP86 functional[48,49] with D3(BJ) correction[50,51] and DZP basis set.[52] Inclusion of dispersion corrections is essential in computational studies of reaction mechanisms involving fullerenes or nanotubes.[53] Solvent effect was treated with the COSMO model[54] applying toluene as solvent with ε=2.38. We checked that solvent was not present inside the SWCNT when performing calculations. QUILD code implemented in ADF was used for stationary points search. Vibrational frequency analysis was performed for all of them. For reactants, intermediates, and products the imaginary frequencies were not found, whereas for transition state structures the only imaginary frequency which reflects the desired transition was detected. Relative Gibbs energies were determined from electronic energies together with corrections of zero-point energies, thermal contributions to the internal energy, and entropy. The structures were visualized with Chemcraft 1.8.[55]

Vertical excitation energies of the BP86-D3(BJ)/DZP structures were calculated using TDA-TDDFT formalism[56] with the range-separated CAM-B3LYP functional[57] and Ahlrichs' Def2-SVP basis set[58,59] including solvent effects of a dichloromethane solution with the COSMO method by means of the Gaussian 16 (rev. A03) program.[60] Full computational details are available in the Supporting Information.

Supporting Information

Optimized structures of (6,5)-SWCNT-TTF complex using 3 and 5 Clar cells models, different orientations of TTF molecule with respect to the nanotube, frontier molecular orbitals representing LE and CT states, excitation energies, dipole moments and solvation energies, HOMO/LUMO

energies for (6,5)-SWCNT–TCAQ complex using 5, 7, 9 and 11 Clar cells models, methodology for investigation of charge-transfer complexes, Cartesian coordinates.

Acknowledgements

We are grateful for financial support from the Spanish MINECO (project CTQ2017-85341-P and Juan de la Cierva formación contracts FJCI-2016-29448 to A.J.S. and FJCI-2017-32757 to O.A.S.), and the Catalan DIUE (2017SGR39). O.A.S and M.S thankfully acknowledge the computer resources at MareNostrum and the technical support provided by Barcelona Supercomputing Center (RES-QS-2019-2-0016).

References

1 Nayak P. K., Mahesh S., Snaith H. J., Cahen K. Photovoltaic solar cell technologies: analysing the state of the art. *Nature Rev. Mat.* **2019**, *4*, 269-285

2 Karousis N., Tagmatarchis N. Current Progress on the Chemical Modification of Carbon Nanotubes. *Chem. Rev.* **2010**, *110*, 5366-5397

3 Zhang X., Hou L., Samorì P. Coupling carbon nanomaterials with photochromic molecules for the generation of optically responsive materials. *Nat. Commun.* **2016**, *7*, 11118

4 Strauss V., Roth A., Sekita M., Guldi D. M. Efficient Energy-Conversion Materials for the Future: Understanding and Tailoring Charge-Transfer Processes in Carbon Nanostructures. *Chem* **2016**, *1*, 531–556

5 Bottari G., Trukhina O., Ince M., Torres T. Towards artificial photosynthesis: supramolecular, donor–acceptor, porphyrin- and phthalocyanine/carbon nanostructure ensembles. *Coord. Chem. Rev.* **2012**, *256*, 2453-2477

6 Umeyama T., Imahori H. Electron transfer and exciplex chemistry of functionalized nanocarbons: effects of electronic coupling and donor dimerization. *Nanoscale Horiz.* **2018**, *3*, 352-366

7 Dirian K., Ángeles Herranz M., Katsukis G., Malig J., Rodríguez-Pérez L., Romero-Nieto C., Strauss V., Martín N., Guldi D. M. Low dimensional nanocarbons – chemistry and energy/electron transfer reactions. *Chem. Sci.* **2013**, *4*, 4335-4353

8 Arellano L. M., Martín-Gomis L., Gobeze H. B., Molina D., Hermosa C., Gómez-Escalonilla M.J., Fierro J. L. G., Sastre-Santos Á., D'Souza F., Langa F. Edge-on and face-on functionalized Pc on enriched semiconducting SWCNT hybrids. *Nanoscale* **2018**, *10*, 5205-5213

9 Roth A., Schierl C., Ferrer-Ruiz A., Minameyer M., Rodríguez-Pérez L., Villegas C., Herranz M. Á., Martín N., Guldi D.M. Low-Dimensional Carbon Allotropes: Groundand Excited-State Charge Transfer with NIRAbsorbing Heptamethine Cyanine. *Chem* **2017**, *3*, 164-173

10 Münich P. W., Schierl C., Dirian K., Volland M., Bauroth S., Wibmer L., Syrgiannis Z., Clark T., Prato M., Guldi D. M. Tuning the Carbon Nanotube Selectivity: Optimizing Reduction Potentials and Distortion Angles in Perylenediimides. *J. Am. Chem. Soc.* **2018**, *140*, 5427-5433

11 Ballesteros B., de la Torre G., Ehli C., Rahman G. M.A., Agulló-Rueda F., Guldi D.M., Torres T. Single-Wall Carbon Nanotubes Bearing Covalently Linked Phthalocyanines − Photoinduced Electron Transfer. *J. Am. Chem. Soc.* **2007**, *129*, 5061–5068

12 Umeyama T., Baek J., Sato Y., Suenaga K., Abou-Chahine F., Tkachenko N. V., Lemmetyinen H., Imahori H. Molecular interactions on single-walled carbon nanotubes revealed by high-resolution transmission microscopy. *Nat. Commun.* **2015**, 6, 7732

13 Bingel C. Cyclopropylation of Fullerenes. *Chem. Ber.* **1993**, *126*, 1957–1959

14 Bolskar R. D., Benedetto A. F., Husebo L. O., Price R.E., Jackson E. F., Wallace S., Wilson L. J., Alford J. M. First Soluble M@C60 Derivatives Provide Enhanced Access to Metallofullerenes and Permit in Vivo Evaluation of Gd@C60[C(COOH)$_2$]10 as a MRI Contrast Agent. *J. Am. Chem. Soc.* **2003**, *125*, 5471-5478

15 Alegret N., Chaur M. N., Santos E., Rodrıguez-Fortea A., Echegoyen L., Poblet J. M. Bingel−Hirsch Reactions on Non-IPR $Gd_3N@C_{2n}$ ($2n$ = 82 and 84). *J. Org. Chem.* **2010**, *75*, 8299–8302

16 Garcia-Borràs M., Cerón M. R., Osuna S., Izquierdo M., Luis J. M., Echegoyen L., Solà M. The Regioselectivity of Bingel-Hirsch Cycloadditions on Isolated Pentagon Rule Endohedral Metallofullerenes. *Angew. Chem. Int. Ed.* **2016**, *55*, 2374-2377

17 Martínez J. P., Garcia-Borràs M., Osuna S., Poater J., Bickelhaupt F. M., Solà M. Reaction Mechanism and Regioselectivity of the Bingel–Hirsch Addition of Dimethyl Bromomalonate to La@C_{2v}-C_{82}. *Chem. Eur. J.* **2016**, *22*, 5953-5962

18 López-Andarias J., Bauzá A., Sakai N., Frontera A., Matile S. Remote Control of Anion–π Catalysis on Fullerene-Centered Catalytic Triads. *Angew. Chem.* **2018**, *130*, 11049-11053

19 Regulska E., Rivera-Nazario D. M., Karpinska J., Plonska-Brzezinska M. E., Echegoyen L. Zinc Porphyrin-Functionalized Fullerenes for the Sensitization of Titania as a Visible-Light Active Photocatalyst: River Waters and Wastewaters Remediation. *Molecules* **2019**, *24*, 1118

20 Besalú-Sala P., Luis J.M., Solà M. Bingel-Hirsch Addition of Diethyl Bromomalonate to Ion-Encapsulated Fullerene M@C_{60} (M = Ø, Li^+, Na^+, K^+, Mg^{+2}, Ca^{+2}, and Cl^-). *Chem. Eur. J.* **2020**, doi:10.1002/chem.202003208.

21 Biglova Y. N., Mustafin A. G. Nucleophilic cyclopropanation of [60]fullerene by the addition–elimination mechanism. *RSC Adv.* **2019**, *9*, 22428-22498

22 Coleman K. S., Bailey S. R., Fogden S., Green M. L. H. Functionalization of Single-Walled Carbon Nanotubes via the Bingel Reaction. *J. Am. Chem. Soc.* **2003**, *125*, 29, 8722-8723

23 Umeyama T., Tezuka N., Fujita M., Matano Y., Takeda N., Murakoshi K., Yoshida K., Isoda S., Imahori H. Retention of Intrinsic Electronic Properties of Soluble Single-Walled Carbon Nanotubes after a Significant Degree of Sidewall Functionalization by the Bingel Reaction. *J. Phys. Chem. C* **2007**, *111*, 9734-9741

24 Betz P., Krueger A. Surface modification of nanodiamond under Bingel-Hirsch conditions. *ChemPhysChem* **2012**, *13*, 2578 – 2584

25 Naebe M., Wang J., Amini A., Khayyam H., Hameed N., Li L. H., Chen Y., Fox B. Mechanical Property and Structure of Covalent Functionalised Graphene/Epoxy Nanocomposites. *Sci. Rep.* **2014**, *4*, 4375

26 Economopoulos S. P., Rotas G., Miyata Y., Shinohara H., Tagmatarchis N. Exfoliation and Chemical Modification Using Microwave Irradiation Affording Highly Functionalized Graphene. *ACS Nano* **2010**, *4*, 7499-7507

27 Economopoulos S. P., Pagona G., Yudasaka M., Iijima S., Tagmatarchis N. Solvent-free microwave-assisted Bingel reaction in carbon nanohorns. *J. Mater. Chem.* **2009**, *19*, 7326-7331

28 Bettinger H. F. Addition of Carbenes to the Sidewalls of Single-Walled Carbon Nanotubes. *Chem. Eur. J.* **2006**, *12*, 4372-4379

29 Lee Y. S., Marzari N. Cycloaddition Functionalizations to Preserve or Control the Conductance of Carbon Nanotubes. *Phys. Rev. Lett.* **2006**, *97*, 116801

30 Lee Y. S., Marzari N. Cycloadditions to Control Bond Breaking in Naphthalenes, Fullerenes, and Carbon Nanotubes: A First-Principles Study. *J. Phys. Chem. C* **2008**, *112*, 4480-4485

31 Lopez-Bezanilla A., Triozon F., Latil S., Blasé X., Roche S. Effect of the Chemical Functionalization on Charge Transport in Carbon Nanotubes at the Mesoscopic Scale. *Nano Lett.* **2009**, *9*, 940-944

32 Li E. Y., Poilvert N., Marzari N. Switchable conductance in functionalized carbon nanotubes via reversible sidewall bond cleavage. *ACS Nano* **2011**, *5*, 4455-4465

33 Baldoni M., Sgamellotti A., Mercuri F. Finite-Length Models of Carbon Nanotubes Based on Clar Sextet Theory. *Org. Lett.* **2007**, *9*, 4267-4270

34 Takano Y., Schubert C., Mizorogi N., Feng L., Iwano A., Katayama M., Ángeles Herranz M., Guldi D. M., Martín N., Nagase S., Akasaka T. Intramolecular *versus* intermolecular electronic interactions between [5,6]-open and [6,6]-closed C_{60} adducts with exTTF. *Chem. Sci.* **2013**, *4*, 3166-3171

35 Cases M., Duran M., Mestres J., Martín N., Solà M. in *Fullerenes for the New Millennium*, ed. P. V. Kamat, K. M. Kadish, D. M. Guldi, The Electrochemical Society Inc., Pennington, vol. 11, 2001, pp. 244-269

36 Umeyama T., Fueno H., Kawabata E., Kobayashi Y., Tanaka K., Tezuka N., Matano Y., Imahori H. Density Functional Theory Studies on Chemical Functionalization of Single-Walled Carbon Nanotubes by Bingel Reaction. *Bull. Chem. Soc. Jpn.* **2011**, *84*, 748-753

37 Martínez J. P., Langa F., Bickelhaupt F. M., Osuna S., Solà M. (4 + 2) and (2 + 2) Cycloadditions of Benzyne to C_{60} and Zig-Zag Single-Walled Carbon Nanotubes: The Effect of the Curvature. *J. Phys. Chem. C* **2016**, *120*, 1716−1726

38 Yang T., Zhao X., Nagase S. Cycloaddition of Benzyne to Armchair Single-Walled Carbon Nanotubes: [2 + 2] or [4 + 2]? *Org. Lett.* **2013**, *15*, 5960−5963

39 Martínez J. P., Vizuete M., Arellano L. M., Poater A., Bickelhaupt F. M., Langa F., Solà M. Regioselectivity of the Pauson-Khand reaction in single-walled carbon nanotubes. *Nanoscale* **2018**, *10*, 15078-15089

40 Miyata Y., Mizuno K., Kataura H. Purity and Defect Characterization of Single-Wall Carbon Nanotubes Using Raman Spectroscopy. *J. Nanomater.* **2011**, *2011*, 786763

41 Kavarnos G. J., Turro N. J. Photosensitization by reversible electron transfer: theories, experimental evidence, and examples. *Chem. Rev.* **1986**, *86*, 401-449

42 Stasyuk A. J., Stasyuk O. A., Solà M., Voityuk A. A. Peculiar Photoinduced Electron Transfer in Porphyrin-Fullerene Akamptisomers. *Chem. Eur. J.* **2019**, *25*, 2577-2585

43 Izquierdo M., Platzer B., Stasyuk A. J., Stasyuk O. A., Voityuk A. A., Cuesta S., Solà M., Guldi D. M., Martín N. All-Fullerene Electron Donor–Acceptor Conjugates. *Angew. Chem. Int. Ed.* **2019**, *58*, 6932-6937

44 Stasyuk A. J., Stasyuk O. A., Solà M., Voityuk A. A. Photoinduced electron transfer and unusual environmental effects in fullerene–Zn-porphyrin–BODIPY triads. *Phys. Chem. Chem. Phys.* **2019**, *21*, 25098-25107

45 Stasyuk A. J., Stasyuk O. A., Filippone S., Martin N., Solà M., Voityuk A. A. Stereocontrolled Photoinduced Electron Transfer in Metal-Fullerene Hybrids *Chem. Eur. J.* **2018**, *24*, 13020-13025

46 ADF 2019.3, SCM, Theoretical Chemistry, Vrije Universiteit, Amsterdam, The Netherlands, http://www.scm.com

47 Swart M., Bickelhaupt F. M. QUILD: QUantum-regions interconnected by local descriptions. *J. Comput. Chem.* **2008**, *29*, 724-734

48 Becke A. D. Density-functional exchange-energy approximation with correct asymptotic behavior. *Phys. Rev. A* **1988**, *38*, 3098-3100

49 Perdew J. P. Density-functional approximation for the correlation energy of the inhomogeneous electron gas. *Phys. Rev. B Condens. Matter.* **1986**, *33*, 8822-8824

50 Grimme S., Antony J., Ehrlich S., Krieg H. A Consistent and Accurate Ab Initio Parametrization of Density Functional Dispersion Correction (DFT-D) for the 94 Elements H-Pu. *J. Chem. Phys.* **2010**, *132*, 154104

51 Grimme S., Ehrlich S., Goerigk L. Effect of the damping function in dispersion corrected density functional theory. *J. Comput. Chem.* **2011**, *32*, 1456-1465

52 van Lenthe E., Baerends E. J. Optimized Slater-type basis sets for the elements 1–118. *J. Comput. Chem.* **2003**, *24*, 1142-1156

53 Osuna S., Swart M., Solà M. Dispersion Corrections Essential for the Study of Chemical Reactivity in Fullerenes. *J. Phys. Chem. A* **2011**, *115*, 3491-3496

54 Pye C. C., Ziegler T. An implementation of the conductor-like screening model of solvation within the Amsterdam density functional package. *Theor. Chem. Acc.* **1999**, *101*, 396-408

55 Zhurko G. A. Chemcraft 1.80 (build 523b) - graphical program for visualization of quantum chemistry computations, https://chemcraftprog.com

56 Hirata S., Head-Gordon M. Time-dependent density functional theory within the Tamm-Dancoff approximation. *Chem. Phys. Lett.* **1999**, *314*, 291-299

57 Yanai T., Tew D. P., Handy N. C. A new hybrid exchange–correlation functional using the Coulomb-attenuating method (CAM-B3LYP). *Chem. Phys. Lett.* **2004**, *393*, 51-57

58 Weigend F., Ahlrichs R. Balanced basis sets of split valence, triple zeta valence and quadruple zeta valence quality for H to Rn: Design and assessment of accuracy. *Phys. Chem. Chem. Phys.* **2005**, ***7***, 3297-3305

59 Weigend F. Accurate Coulomb-fitting basis sets for H to Rn. *Phys. Chem. Chem. Phys.* **2006,** *8*, 1057-1065

60 Gaussian 16, Revision A.03, Frisch, M. J.; Trucks, G. W.; Schlegel, H. B.; Scuseria, G. E.; Robb, M. A.; Cheeseman, J. R.; Scalmani, G.; Barone, V.; Petersson, G. A.; Nakatsuji, H.; Li, X.; Caricato, M.; Marenich, A. V.; Bloino, J.; Janesko, B. G.; Gomperts, R.; Mennucci, B.; Hratchian, H. P.; Ortiz, J. V.; Izmaylov, A. F.; Sonnenberg, J. L.; Williams-Young, D.; Ding, F.; Lipparini, F.; Egidi, F.; Goings, J.; Peng, B.; Petrone, A.; Henderson, T.; Ranasinghe, D.; Zakrzewski, V. G.; Gao, J.; Rega, N.; Zheng, G.; Liang, W.; Hada, M.; Ehara, M.; Toyota, K.; Fukuda, R.; Hasegawa, J.; Ishida, M.; Nakajima, T.; Honda, Y.; Kitao, O.; Nakai, H.; Vreven, T.; Throssell, K.; Montgomery, J. A., Jr.; Peralta, J. E.; Ogliaro, F.; Bearpark, M. J.; Heyd, J. J.; Brothers, E. N.; Kudin, K. N.; Staroverov, V. N.; Keith, T. A.; Kobayashi, R.; Normand, J.; Raghavachari, K.; Rendell, A. P.; Burant, J. C.; Iyengar, S. S.; Tomasi, J.; Cossi, M.; Millam, J. M.; Klene, M.; Adamo, C.; Cammi, R.; Ochterski, J. W.; Martin, R. L.; Morokuma, K.; Farkas, O.; Foresman, J. B.; Fox, D. J. Gaussian, Inc., Wallingford CT, 2016